A Nonlinear Extended State Observer Design for Torsional Vibrations Estimation in PMSM Drive

Matteo Deponti
Energy Department (DENG),
Politecnico di Milano
Milano, Italy
matteo.deponti@polimi.it

Dejan Pejovski
Energy Department (DENG),
Politecnico di Milano
Milano, Italy
dejan.pejovski@polimi.it

Antonino Di Gerlando
Energy Department (DENG),
Politecnico di Milano
Milano, Italy
antonino.digerlando@polimi.it

Roberto Perini
Energy Department (DENG),
Politecnico di Milano
Milano, Italy
roberto.perini@polimi.it

***Abstract*— In every drivetrain, torque harmonics coming from electrical and mechanical sources lead to torsional vibrations. In this paper, a Nonlinear Extended State Observer (NESO) is designed to estimate the shaft torque in a Two Degree-of-Freedom (DOF) system, comprising a Permanent Magnet Synchronous Machine (PMSM), an elastic shaft, a rotating load. The system is modeled as a Multi-Input Multi-Output (MIMO) nonlinear system. Being the NESO commonly defined for single-output systems, a procedure to implement it for the MIMO nonlinear system under consideration is presented. Moreover, a general method to transform a generic MIMO system into an integral-chain form is provided, enabling NESO application. The observer performance is evaluated through computer simulations.**

Keywords*— *Nonlinear, State Observer, Extended State Observer, Multi-Input Multi-Output, MIMO, Torsional, Vibrations, PMSM

I. INTRODUCTION

In every drivetrain, the shaft finite stiffness allows torsional oscillations between each rotating mass: if a torsional natural frequency is excited by an external force or disturbance, a mechanical resonance occurs. Without a proper mitigation technique, torsional vibrations cause not only fatigue stress in the drivetrain and reliability issues [1], [2], but also additional electrical losses and temperature rise in the electrical machine [3]. In an electric drivetrain, these vibrations are mainly caused by voltage and current harmonics, for example, due to the switching operation of the Voltage Source Converter (VSC) [4] or slot-harmonics [2], as well as by mechanical disturbances such as frictional torque from the drivetrain bearings or gearbox [1], [5]. The measurement or estimation of torsional vibrations can be done in different ways. One is by measurement of the shaft torque, through optical sensors or strain gauges (or torque meters) mounted on the shaft; however, in addition to higher costs, the installation of this type of sensors may not be possible owing to lack of space or inaccessibility. Another way is to estimate torsional oscillations through the so-called Motor Current Signature Analysis (MCSA) [6], [7], [8], although other disturbances can be superimposed on the torsional vibration-related information of the measured electrical quantities, leading to more complex estimation algorithms. A promising way for the online estimation of torsional vibrations is represented by a model-based estimation implementing a State Observer (SO). In [9] and [10], different SOs are tested and compared on a common simulation testbench. To overcome the problem of the classical Luenberger Observer (LO), being too susceptible to the system parameters' inaccuracies and disturbances, other structures can be used. The High Gain Observer (HGO), defined in [11] for a class of nonlinear systems where the state variables' nonlinear function is related to the system output, as well as the Sliding-Mode Observer (SMO) are more robust to the system noises and disturbances. On the other hand, the Extended State Observer (ESO) [12] is independent of the system parameters, as well as robust against unknown disturbances and noises. In [9], the Nonlinear Extended State Observer (NESO), which is an ESO with a nonlinear gain function, shows better performance compared to SMO and HGO on the same testbench. In [13], an NESO is implemented to estimate stator currents and back-EMF of a Permanent Magnet Synchronous Motor (PMSM) Brushless DC drive. In [14], an advanced control algorithm based on an NESO is used to damp torsional oscillations in a wind turbine drivetrain, starting from a nonlinear system and applying a Brunowski Form transformation. However, most of the work present in the literature deals with Single-Output systems, where only one measured variable is used as input for the observer.

This paper proposes a novel NESO design for the estimation of torsional vibrations in a two-mass PMSM drivetrain. The system is modeled considering both the mechanical and electrical dynamics to exploit all the available system data, leading to a Multi-Input Multi-Output (MIMO) nonlinear system definition. Being the NESO commonly defined for single-output systems, a procedure to implement it for the multi-output nonlinear system under consideration is presented. Furthermore, a general method to transform a generic Multi-Input Single-Output system into an integral chain form is provided, which enables NESO application. Summarizing, the main contributions of this paper are:

- definition of an all-inclusive multi-input multi-output nonlinear model comprising the system mechanical and electrical dynamics;
- simple and comprehensive step-by-step procedure for NESO definition for a nonlinear MIMO system.

This work is organized as follows: Section II is dedicated to the two-mass MIMO system definition; Section III introduces the formulation of the NESO and its design for the system under study; in Section IV the proposed observer is tested in a Matlab/Simulink environment, showing the

observer effectiveness in estimating high and low amplitude torsional vibrations; Section V is reserved for conclusion.

II. System Definition

A. Two-Degree-of-Freedom (DOF) PMSM drive

The system under analysis comprises a PMSM connected through a shaft to a generic load, as shown in Fig. 1. The finite shaft stiffness is denoted as K_{sh}, and the load torque is assumed controlled to be proportional to the load speed: $T_L = K_L\,\Omega_L$.

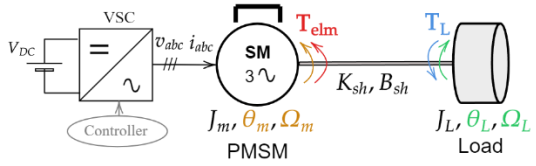

Fig. 1. Simplified scheme of the PMSM Two-Degree-of-Freedom system

The motor is fed by a PWM VSC with a constant switching frequency f_{sw}. The system is controlled by means of an internal d-q current PI control loop, based on the Maximum Torque per Ampere (MTPA) technique, and an external speed PI control loop. The two-DOF PMSM drive is modeled through a system of six first-order differential equations comprising both the mechanical and the electrical models, the latter one in the d-q reference frame. Both models are referred to as p.u. (per unit) variables. In this work, the observer is supposed to be operating in open-loop, without feedback of the estimates to the control system. For this reason, the control dynamics are not affected by the observer, thus it is not included in the model.

B. Mechanical model

The mechanical model in p.u is based on the second Newton's law applied to both masses, hence:

$$\begin{cases} \dfrac{J_m}{T_{nm}} p\Omega_m = 2H_m p\omega_m = -\dfrac{T_{sh}}{T_{nm}} + \dfrac{T_{elm}}{T_{nm}} \\ \dfrac{J_L}{T_{nL}} p\Omega_L = 2H_L p\omega_L = \dfrac{T_{sh}}{T_{nL}} - \dfrac{T_L}{T_{nL}} \end{cases} \quad (1)$$

where:

- Ω_m,Ω_L/ω_m,ω_L are the mechanical speeds in absolute value and in p.u.;
- $p = d/dt$: derivative operator;
- $\Omega_{b,mech} = \Omega_{n,m}$: base mechanical speed;
- $T_{sh} = K_{sh}(\theta_m - \theta_L) + B_{sh}(\Omega_m - \Omega_L)$: shaft torque, where B_{sh} is the shaft damping coefficient;
- J_m and J_L are the motor and load moments of inertia;
- T_{nm} and T_{nL}: motor and load nominal torques;
- $H_m = 0.5 * \frac{J_m\,\Omega_{b,mech}^2}{T_{nm}\,\Omega_{b,mech}}$, motor inertia constant;
- $H_L = 0.5 * \frac{J_L\,\Omega_{b,mech}^2}{T_{nL}\,\Omega_{b,mech}}$, load inertia constant;
- T_{elm} and T_L are the motor and load torques.

In the following, $B_{sh}(\Omega_m - \Omega_L)$ will be neglected, its value being considerably smaller than the other terms in the equation. The mechanical parameters are listed in TABLE I (see Appendix II).

C. Electrical model

The electrical model in p.u. is based on the PMSM stator voltage equations in d-q reference frame, that are:

$$\begin{cases} v_{sd} = r_s i_{sd} + \dfrac{l_s}{\omega_b} p i_{sd} - l_s \omega_m i_{sq} \\ v_{sq} = r_s i_{sq} + \dfrac{l_s}{\omega_b} p i_{sq} + l_s \omega_m i_{sd} + \omega_m \psi_{pm,q} \end{cases} \quad (2)$$

System (2) was obtained considering a power invariant reference frame transformation and the following p.u. base values:

- $V_{b,dq} = \sqrt{3} V_{n,phase}$; $I_{b,dq} = \sqrt{3} I_{n,abc}$;
- $\omega_b = pp * \Omega_{b,mech}$; $\Psi_b = V_b/\omega_b$; pp: pole pairs;
- $T_b = pp * I_b * \psi_b$;
- $Z_b = V_{b,dq}/I_{b,dq}$ and $L_b = Z_b/\omega_b$.

The PMSM electrical parameters are listed in TABLE I.

D. System in State Space form

Consider that:

- $T_{elm} = \psi_{pm,q} i_{sq} T_b$;
- T_L, v_{sd} and v_{sq} are system inputs;
- θ_m, i_{sd} and i_{sq} are assumed to be measured system outputs.

By merging (1) and (2), rearranging the terms to make the derivative of the state variables explicit, and denoting the measured variables with the letter y, the nonlinear MIMO system in state-space form shown in (3) is obtained.

$$\begin{cases} p\theta_m = \Omega_{b,mech}\omega_m \\ p\theta_L = \Omega_{b,mech}\omega_L \\ p\omega_m = -\dfrac{K_{sh}}{2H_m T_{nm}}(\theta_m - \theta_L) + \dfrac{\psi_{pm,q} T_b}{2H_m T_{nm}} i_{sq} \\ p\omega_L = \dfrac{K_{sh}}{2H_L T_{nL}}(\theta_m - \theta_L) - \dfrac{T_L}{2H_L T_{nL}} \\ p i_{sd} = -\dfrac{r_s \omega_b}{l_s} i_{sd} + \omega_b i_{sq} \omega_m + \dfrac{\omega_b}{l_s} v_{sd} \\ p i_{sq} = -\dfrac{r_s \omega_b}{l_s} i_{sq} - \omega_b i_{sd} \omega_m - \dfrac{\omega_b}{l_s} \psi_{pm,q} \omega_m + \dfrac{\omega_b}{l_s} v_{sq} \\ y_1 = \theta_m \\ y_2 = i_{sd} \\ y_3 = i_{sq} \end{cases} \quad (3)$$

The nonlinear terms are given by the multiplication between the state variables present in the d-q current differential equation, thus by $i_{sd}\omega_m$ and $i_{sq}\omega_m$. The magnitude of the shaft torque $T_{sh} = K_{sh}(\theta_m - \theta_L)$ represents a good indicator of torsional vibrations intensity: while θ_m is measured, θ_L will be estimated by the NESO. The observer performance will be evaluated based on its accuracy at estimating T_{sh} magnitude, directly related to θ_L estimation.

III. Nonlinear Extended State Observer (NESO)

A. Definition

Consider a generic observable Single Input Single Output (SISO) system in integral chain form:

$$\begin{cases} px_1 = x_2 \\ px_2 = x_3 \\ \dots \\ px_n = f(x_1, x_2, \dots, x_n) + w + u \\ y = x_1 \end{cases} \quad (4)$$

where $w(t) \in R$ is an unknown disturbance, u is the system input and $f: R^n \to R$ is an unknown function. Defining an additional state variable x_{n+1} and its derivative:

$$\begin{cases} x_{n+1} = f(x_1, x_2, \dots, x_n) + w \\ px_{n+1} = h \end{cases} \quad (5)$$

and substituting (5) into (4), an NESO can be defined as:

$$\begin{cases} p\hat{x}_1 = \hat{x}_2 - \beta_1 g(\hat{y} - y) \\ p\hat{x}_2 = \hat{x}_3 - \beta_2 g(\hat{y} - y) \\ \dots \\ p\hat{x}_n = \hat{x}_{n+1} + u - \beta_n g(\hat{y} - y) \\ p\hat{x}_{n+1} = \hat{h} - \beta_{n+1} g(\hat{y} - y) \\ \hat{y} = \hat{x}_1 \end{cases} \quad (6)$$

where $\beta_i \mid i = 1, \dots, n, n+1$ are the observer gain coefficients and $g: R \to R$ is a generic nonlinear function [12]. The hats above the state variables denote that they are estimates. Since the system represented by (3) is nonlinear and MIMO, the NESO defined in (6) cannot be applied straightforwardly. In the following, a procedure to design an NESO for (3) is presented.

B. System linearisation

As previously stated, the main goal of the observer is to estimate torsional vibrations, which are inherently oscillating phenomena. Applying the small signal analysis, the generic state variable $x(t)$ can be seen as $x(t) = x_0 + \Delta x(t)$, where x_0 is a constant steady-state value and $\Delta x(t)$ represents a small perturbation. Apply this concept also to the system inputs and outputs of (3) and consider:

- $\Delta x_i * \Delta x_j \approx 0 \mid \forall i, j$;
- $i_{sd0} \approx 0$ (MTPA control technique), $i_{sq0} = \frac{T_{n,m}}{\psi_{pm,q} T_b}$; $\omega_{m0} = \frac{\Omega_{n,m}}{\Omega_{b,mech}} = 1$.

Finally, system (3) can be split into a steady-state constant system and a linear Δ dynamic one; the latter one in matrix form:

$$\begin{aligned} p\boldsymbol{\Delta x} &= \boldsymbol{A_\Delta \Delta x} + \boldsymbol{B_\Delta \Delta u} \\ \boldsymbol{\Delta y} &= \boldsymbol{C_\Delta \Delta x} \end{aligned} \quad (7)$$

where:

- $\boldsymbol{A_\Delta} = \begin{bmatrix} 0 & 0 & a_{13} & 0 & 0 & 0 \\ 0 & 0 & 0 & a_{24} & 0 & 0 \\ a_{31} & a_{32} & 0 & 0 & 0 & a_{36} \\ a_{41} & a_{42} & 0 & 0 & 0 & 0 \\ 0 & 0 & a_{53} & 0 & a_{55} & a_{56} \\ 0 & 0 & a_{63} & 0 & a_{65} & a_{66} \end{bmatrix} \in R^{nxn}$

$$a_{13} = a_{24} = \Omega_{b,mech}; a_{31} = a_{42} = -\frac{K_{sh}}{2H_m T_{nm}};$$

$$a_{32} = a_{41} = \frac{K_{sh}}{2H_m T_{nm}}; a_{36} = \frac{\psi_{pm,q} T_b}{2H_m T_{nm}};$$

$$a_{53} = \omega_b i_{sq0}; a_{55} = -\frac{r_s \omega_b}{l_s}; a_{56} = -a_{65} = \omega_b \omega_{m0};$$

$$a_{63} = -\omega_b i_{sd0} - \frac{\omega_b}{l_s}\psi_{pm,q}; a_{66} = -\frac{r_s \omega_b}{l_s};$$

- $\boldsymbol{B_\Delta} = \begin{bmatrix} 0 & 0 & 0 & -\frac{1}{2H_L T_{nL}} & 0 & 0 \\ 0 & 0 & 0 & 0 & \frac{\omega_b}{ls} & 0 \\ 0 & 0 & 0 & 0 & 0 & \frac{\omega_b}{ls} \end{bmatrix}^T \in R^{nxp}$;
- $\boldsymbol{C_\Delta} = \begin{bmatrix} 1 & 0 & 0 & 0 & 0 & 0 \\ 0 & 0 & 0 & 0 & 1 & 0 \\ 0 & 0 & 0 & 0 & 0 & 1 \end{bmatrix} \in R^{qxn}$;
- $\boldsymbol{\Delta x} = \left[\Delta\theta_m \; \Delta\theta_L \; \Delta\omega_m \; \Delta\omega_L \; \Delta i_{sd} \; \Delta i_{sq}\right]^T$;
- $\boldsymbol{\Delta u} = \left[\Delta v_{sd} \; \Delta v_{sq} \; \Delta T_L\right]^T$;

with $n = 6$ states, $p = 3$ inputs and $q = 3$ outputs.

C. Subsystem decomposition

To design an NESO of the form (6), the system needs to be an observable single-output system, while (7) is multi-output. For this reason, the system is decomposed into $q = 3$ single-output subsystems, equal to the number of outputs: the idea is to design an NESO for each subsystem. Keeping the same state vector $\boldsymbol{\Delta x} \in R^n$ and matrices $\boldsymbol{A_\Delta} \in R^{nxn}$ and $\boldsymbol{B_\Delta} \in R^{nxp}$, three subsystems differing only in the output matrix are created:

- Subsystem 1: $\boldsymbol{C_{\Delta 1}} = [1\ 0\ 0\ 0\ 0\ 0]$;
- Subsystem 2: $\boldsymbol{C_{\Delta 2}} = [0\ 0\ 0\ 0\ 1\ 0]$;
- Subsystem 3: $\boldsymbol{C_{\Delta 3}} = [0\ 0\ 0\ 0\ 0\ 1]$;

The observability of the pair $(\boldsymbol{C_{\Delta i}}, \boldsymbol{A_\Delta})$ of the generic subsystem i must be evaluated, being a necessary condition for the state observer design. Recalling that the subsystem i is observable if the rank of the observability matrix $\boldsymbol{M_{Oi}} = \left[\boldsymbol{C_{\Delta i}} \; \boldsymbol{C_{\Delta i} A_\Delta} \dots \boldsymbol{C_{\Delta i}} \boldsymbol{A_\Delta^{n_i}}\right]^T$ is equal to the number of its state variables n_i [15], this analysis leads to:

- Subsystem 1: $rank(\boldsymbol{M_{O1}}) = 6 = n_i = n$;
- Subsystem 2: $rank(\boldsymbol{M_{O2}}) = 5 \neq n_i = n$;
- Subsystem 3: $rank(\boldsymbol{M_{O3}}) = 5 \neq n_i = n$.

As can be seen, the observability condition is not satisfied for subsystems 2 and 3, as they contain non-observable state variables. For a generic linear time-invariant state-space system, the non-observable states subspace $\boldsymbol{x_{null}}$ is identified by calculating the kernel of $\boldsymbol{M_O}$ [16]. In this case, through a Matlab script, it can be found that $\ker(\boldsymbol{M_{O1}}) = \ker(\boldsymbol{M_{O2}}) = [1\ 1\ 0\ 0\ 0\ 0]^T$. Apparently, the non-observable states of subsystems 2 and 3 are represented by $\Delta\theta_m$ and $\Delta\theta_L$, i.e. the state variables occupying the position of the non-null elements in $\ker(\boldsymbol{M_{O1}}), \ker(\boldsymbol{M_{O2}})$. As a first attempt to satisfy the observability requirement, the state variables of the non-observable subsystems are rearranged by merging $\Delta\theta_m$ and $\Delta\theta_L$ in a unique state variable: $\Delta\theta_m - \Delta\theta_L$. It follows that, for subsystems 2 and 3, the state variables vectors become $\boldsymbol{\Delta x_2} = \boldsymbol{\Delta x_3} \in R^{n-1} \neq \boldsymbol{\Delta x}$, leading to $\boldsymbol{A_{\Delta 2}} = \boldsymbol{A_{\Delta 3}} \neq \boldsymbol{A_\Delta}$ and $\boldsymbol{B_{\Delta 2}} = \boldsymbol{B_{\Delta 3}} \neq \boldsymbol{B_\Delta}$. Now, evaluating the observability of the re-configured Subsystems 2 and 3, results in:

- Subsystem 2: $rank(\boldsymbol{M_{O2}}') = 5 = n_2 = n - 1$;

- Subsystem 3: $rank(\boldsymbol{M_{O3}}') = 5 = n_3 = n - 1$;

that proves their observability. Finally, three observable single-output subsystems are obtained:

- Subsystem 1:

$$\boldsymbol{\Delta x_1} = \boldsymbol{\Delta x};\ \boldsymbol{\Delta u_1} = \boldsymbol{\Delta u};\ \boldsymbol{A_{\Delta 1}} = \boldsymbol{A_\Delta};\ \boldsymbol{B_{\Delta 1}} = \boldsymbol{B_\Delta};$$
$$\boldsymbol{C_{\Delta 1}} = [1\ 0\ 0\ 0\ 0\ 0];$$

- Subsystem 2:

$$\boldsymbol{\Delta x_2} = \left[(\Delta\theta_m - \Delta\theta_L)\ \Delta\omega_m\ \Delta\omega_L\ \Delta i_{sd}\ \Delta i_{sq}\right]^T; \boldsymbol{\Delta u_2} = \boldsymbol{\Delta u};$$

$$\boldsymbol{A_{\Delta 2}} = \begin{bmatrix} 0 & a_{13} & -a_{24} & 0 & 0 \\ a_{31} & 0 & 0 & 0 & a_{36} \\ a_{41} & 0 & 0 & 0 & 0 \\ 0 & a_{53} & 0 & a_{55} & a_{56} \\ 0 & a_{63} & 0 & a_{65} & a_{66} \end{bmatrix};$$

$$\boldsymbol{B_{\Delta 2}} = \begin{bmatrix} 0 & 0 & -\dfrac{1}{2H_L T_{nL}} & 0 & 0 \\ 0 & 0 & 0 & \dfrac{\Omega_b}{ls} & 0 \\ 0 & 0 & 0 & 0 & \dfrac{\Omega_b}{ls} \end{bmatrix}^T;$$

$$\boldsymbol{C_{\Delta 2}} = [0\quad 0\quad 0\quad 1\quad 0];$$

- Subsystem 3:

$$\boldsymbol{\Delta x_3} = \boldsymbol{\Delta x_2}; \boldsymbol{\Delta u_3} = \boldsymbol{\Delta u}; \boldsymbol{A_{\Delta 3}} = \boldsymbol{A_{\Delta 2}};\ \boldsymbol{B_{\Delta 3}} = \boldsymbol{B_{\Delta 2}};$$
$$\boldsymbol{C_{\Delta 3}} = [0\quad 0\quad 0\quad 0\quad 1];$$

D. Integral chain form transformations

As already mentioned, the NESO needs the system to be in integral-chain form. To accomplish this, a linear transformation of the state variables $\boldsymbol{\Delta z_i} = \boldsymbol{T_i}\boldsymbol{\Delta x_i}$ is applied to each subsystem $i = 1,2,3$, which transforms each subsystem into the realization of the observability canonical form. Consider the generic subsystem i:

$$\begin{aligned} p\boldsymbol{\Delta x_i} &= \boldsymbol{A_{\Delta i}}\boldsymbol{\Delta x_i} + \boldsymbol{B_{\Delta i}}\boldsymbol{\Delta u} \\ \Delta y_i &= \boldsymbol{C_{\Delta i}}\boldsymbol{\Delta x_i} \mid i = 1,2,3 \end{aligned} \tag{8}$$

with $\boldsymbol{A_{\Delta i}} \in R^{n_i x n_i}$, $\boldsymbol{B_{\Delta i}} \in R^{n_i x p}$, $\boldsymbol{C_{\Delta i}} \in R^{1 x n_i}$, $n_1 = 6$, $n_2 = n_3 = 5$, $p = 3$. The transformed Subsystem i becomes:

$$\begin{aligned} p\boldsymbol{\Delta z_i} &= \boldsymbol{A_{zi}}\boldsymbol{\Delta z_i} + \boldsymbol{B_{zi}}\boldsymbol{\Delta u} \\ \Delta y_{z,i} &= \Delta y_i = \boldsymbol{C_{zi}}\boldsymbol{\Delta z} = \boldsymbol{C_{\Delta i}}\boldsymbol{\Delta x_i} \end{aligned} \tag{9}$$

The procedure to find the Subsystem i transformation matrix $\boldsymbol{T_i}$ is presented in Appendix I; once it is found, the following holds: $\boldsymbol{A_{zi}} = \boldsymbol{T_i}\boldsymbol{A_{\Delta i}}\boldsymbol{T_i^{-1}}$, $\boldsymbol{B_{zi}} = \boldsymbol{T_i}\boldsymbol{B_{\Delta i}}$, $\boldsymbol{C_{zi}} = \boldsymbol{C_{\Delta i}}\boldsymbol{T_i^{-1}}$.

E. NESO design

The last step is to apply the definition of NESO (6) to the transformed subsystem $i = 1,2,3$ (9), as can be seen in (10), with $n_1 = n = 6$ for subsystem 1 and $n_2 = n_3 = 5$ for subsystems 2 and 3. The definition of $\Delta\hat{z}_{i,n_i+1}$ represents the main advantage of this observer: all the dynamic elements of the system are contained in the extended state $\Delta z_{i,n_i+1}$, thus the observer performance is independent of the former system parameters.

$$\begin{cases} p\Delta\hat{z}_{i,1} = \Delta\hat{z}_{i,2} + B_{zi,11}\Delta u_1 + B_{zi,12}\Delta u_2 + B_{zi,13}\Delta u_3 - \\ \qquad -\beta_1 g(\Delta\hat{z}_{i,1} - \Delta z_{i,1}) \\ p\Delta\hat{z}_{i,2} = \Delta\hat{z}_{i,3} + B_{zi,21}\Delta u_1 + B_{zi,22}\Delta u_2 + B_{zi,23}\Delta u_3 - \\ \qquad -\beta_2 g(\Delta\hat{z}_{i,1} - \Delta z_{i,1}) \\ \qquad \cdots \\ p\Delta\hat{z}_{i,n_i} = \Delta\hat{z}_{i,n_i+1} + B_{zi,n_i1}\Delta u_1 + B_{zi,n_i2}\Delta u_2 + B_{zi,n_i3}\Delta u_3 - \\ \qquad -\beta_{n_i} g(\Delta\hat{z}_{i,1} - \Delta z_{i,1}) \\ p\Delta\hat{z}_{i,n_i+1} = \widehat{h_i} - \beta_{n_i+1} g(\Delta\hat{z}_{i,1} - \Delta z_{i,1}) \\ \Delta\hat{y}_{zi} = \Delta\hat{z}_{i,1} = \Delta y_i \\ where:\ \Delta\hat{z}_{i,n_i+1} = A_{zi,1}\Delta\hat{z}_{i,1} + \cdots + A_{zi,n_i}\Delta\hat{z}_{i,n_i}. \end{cases} \tag{10}$$

The observer correction term is defined by a β-coefficient that multiplies a nonlinear function $g(.): R \to R$ of the observation error $e_{i,1} = \Delta\hat{z}_{i,1} - \Delta z_{i,1}$, which was chosen to be the so-called fal-function defined as:

$$fal(\alpha, \delta, x) = \begin{cases} \dfrac{x}{\delta^{1-\alpha}}, & |x| \le \delta \\ |x|^\alpha sign(x), & |x| > \delta \end{cases} \tag{11}$$

with $\alpha, \delta \in R$ to be selected based on the desired observer response. An analysis of the impact of α and δ on the shape of $fal(\alpha, \delta, x)$ is provided in [13], where the gain function $F(\alpha, \delta, x) = fal(\alpha, \delta, x)/x$ is analyzed. Choosing δ close to one widens the constant gain part of $F(\alpha, \delta, x)$, i.e. when $|x| \le \delta$, decreasing its value; it has no effect on $F(\alpha, \delta, x)$ for $|x| > \delta$. On the other hand, a small value of α increases the constant gain value for $|x| \le \delta$, while it lowers $|F(\alpha, \delta, x)|$ for $|x| \gg \delta$. In this work, $\alpha = 0.65$ and $\delta = 0.9$ were chosen, based on a trial-and-error approach: $g(\alpha, \delta, e_{i,1})$ and $F(\alpha, \delta, e_{i,1})$ are shown in Fig. 2.

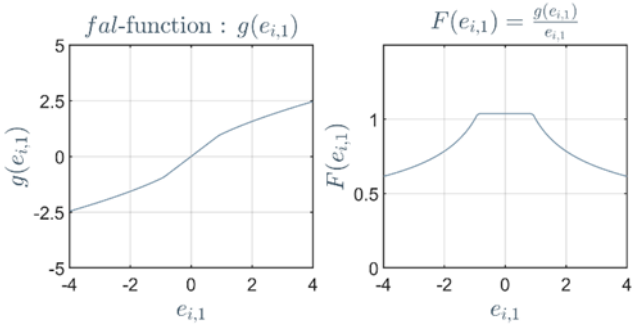

Fig. 2. Plots of $g(e_{i,1}) = fal(\alpha, \delta, x)$ and $F(e_{i,1}) = g(e_{i,1})/e_{i,1}$; δ is related to the plateau width and amplitude in $F(e_{i,1})$; α affects both magnitude and slope of $F(e_{i,1})$

As can be seen from the $F(\alpha, \delta, e_{i,1})$ trend, the nonlinear function provides a constant gain close to unity for small values of the error, i.e. for $|e_{i,1}| \le \delta = 0.9$, while it decreases the gain as $e_{i,1}$ increases. Let us define the observation error system considering $\boldsymbol{e_i} = \boldsymbol{\Delta\hat{z}_i} - \boldsymbol{\Delta z_i}$:

$$\begin{cases} pe_{i,1} = e_{i,2} - \beta_1 g(e_{i,1}) \\ pe_{i,2} = e_{i,3} - \beta_2 g(e_{i,1}) \\ \qquad \cdots \\ pe_{i,n_i} = e_{i,n_i+1} - \beta_{n_i} g(e_{i,1}) \\ pe_{i,n_i+1} = (\widehat{h_i} - h_i) - \beta_{n_i+1} g(e_{i,1}) \end{cases} \tag{12}$$

The choice of the β-coefficients is based on a direct pole-placement approach. Assuming that $e_{i,1}$ keeps a small value, i.e. the observation error of the measured state variable is low in magnitude, $fal(\alpha, \delta, e_{i,1})$ can be seen as defined in the first row of (11), i.e. as a linear function. This does not represent

a strong assumption: in fact, in a system defined in p. u., $e_{i,1}$ has rather low magnitude, hence less than $\delta = 0.9$. Hence, (12) becomes:

$$\begin{cases} pe_{i,1} = e_{i,2} - \beta_1 K_{\delta,\alpha} e_{i,1} \\ pe_{i,2} = e_{i,3} - \beta_2 K_{\delta,\alpha} e_{i,1} \\ \dots \\ pe_{i,n_i} = e_{i,n_i+1} - \beta_{n_i} K_{\delta,\alpha} e_{i,1} \\ pe_{i,n_i+1} = (\hat{h}_i - h_i) - \beta_{n_i+1} K_{\delta,\alpha} e_{i,1} \end{cases} \quad (13)$$

where $K_{\delta,\alpha} = \frac{1}{\delta^{1-\alpha}}$. Neglecting the observation disturbance term $\hat{h} - h$ assuming it is bounded, (13) can be seen as a linear dynamic system $p\boldsymbol{e_i} = \boldsymbol{A_{ei}} \boldsymbol{e_i}$. The poles of (13) are placed all equal and real, solving: $\det(s\boldsymbol{I} - \boldsymbol{A_{ei}}) = (s + \alpha_0)^{n_i+1} \mid \alpha_0 = \frac{1}{10} \frac{2\pi}{h_{step}}$, where h_{step} is the integration step of the microcontroller. Some considerations about the pole location choice:

- in this system, each state observer outputs, i.e. its estimates, are not used by the control system: hence, the choice of its poles is purely based on the desired observation errors' dynamics;
- the only limitation is the computational speed of the microcontroller, this is why the poles are located with a natural frequency ten times slower than the microcontroller one.

The described methodology is applied to each of the $q = 3$ subsystems; the β-coefficients are listed in TABLE III.

F. State estimates selection

In a practical setup, the state observer is implemented on a microcontroller and operates in the discrete-time domain. Therefore, if an NESO is designed for each of the $q = 3$ subsystems, q sets of state variables estimates are generated at each time step k. The calculation of the state variables best estimates out of the three available sets must be assessed. To do this, a Least-Mean Square Error (LMSE)-based approach is used. Let us consider the generic state variable $\Delta x(k)$ at time step k, and define with $\Delta\hat{x}_i(k)$ its estimate generated from Subsystem $i = 1,2,3$; the following holds:

$$\begin{bmatrix} e_1(k) \\ e_2(k) \\ e_3(k) \end{bmatrix} = \boldsymbol{e}(k) = \begin{bmatrix} \Delta\hat{x}_1(k) \\ \Delta\hat{x}_2(k) \\ \Delta\hat{x}_3(k) \end{bmatrix} - \begin{bmatrix} \Delta x(k) \\ \Delta x(k) \\ \Delta x(k) \end{bmatrix} \quad (14)$$

Let us denote with K the total number of samples acquired in a limited time window, and define $J(\Delta x(k), k) = \boldsymbol{e}(k)^{\boldsymbol{T}} \boldsymbol{W} \boldsymbol{e}(k)$, where $\boldsymbol{W}$ is the weight matrix:

$$\boldsymbol{W} = \frac{1}{w_1 + w_2 + w_3} * \begin{bmatrix} w_1 & 0 & 0 \\ 0 & w_2 & 0 \\ 0 & 0 & w_3 \end{bmatrix} \quad (15)$$

with $w_1, w_2. w_3 \in [-1,1]$ and $w_1 + w_2 + w_3 \neq 0$. The idea is to find $\boldsymbol{W}$ that minimizes J_{LMS} defined as:

$$J_{LMS} = \sum_{k=1}^{K} |J(\Delta x(k), k)| \quad (16)$$

Some considerations can be made:

- since the true state variable $\Delta x(k)$ changes at every step following the system dynamics, a single choice of $\boldsymbol{W}$ may not minimize J_{LMS} for any set of arbitrary K samples acquired. However, one can choose $\boldsymbol{W}$ that minimizes J_{LMS} at a specific operating condition, as will be seen in Section IV;
- the information on the non-measured state variables is not available in an experimental setup: the optimal weights are computed offline relying merely on the simulation results;
- the choice of the number of samples K is arbitrary and should be enough to contain the information of the error periodical time-variation.

Finally, after computing $\boldsymbol{W}$, at each time step k the generic state variable estimate $\Delta\hat{x}(k)$ is calculated through: $\Delta\hat{x}(k) = \text{diag}\{\boldsymbol{W}\} * \boldsymbol{\Delta\hat{x}}(k) \mid \boldsymbol{\Delta\hat{x}}(k) = [\Delta\hat{x}_1(k)\ \Delta\hat{x}_2(k)\ \Delta\hat{x}_3(k)]^T$, with $\text{diag}\{\boldsymbol{W}\} \in R^{1x3}$.

IV. Simulation results

A. Simulation setup

The objective of the simulation is to assess the estimation performance of the observer under strong torsional vibrations, hence at mechanical resonance. The simulation is performed in a Matlab/Simulink environment. The voltage harmonic components able to produce a torque harmonic inside the machine are those of orders $6k \pm 1 \mid k \in N$, leading to torque harmonics of order $6k$. Hence, two types of low-frequency voltage harmonics are superimposed on the PMSM terminal voltages:

- One of order $h_{13} = 13$ (positive sequence), responsible for a torque harmonic of order $h_{13} - 1$ leading to a mechanical resonance at $\omega_m^{res,h_{13}} = \frac{\omega_{res}}{(h_{13}-1)*pp} = 87.8 * 10^{-3}$ p. u., where $\omega_{res} = \frac{\Omega_{res}}{\Omega_{b,mech}}$;
- One of order $h_5 = 5$ (negative sequence), responsible for a torque harmonic of order $h_5 + 1$ leading to a mechanical resonance at $\omega_m^{res,h_5} = \frac{\omega_{res}}{(h_5+1)*pp} = 0.17$ p. u..

These voltage harmonics orders may be present in the voltage spectrum of a generic PMSM, for example in the case of square wave or overmodulation PWM technique, small values of m_f in linear PWM, but also because of machine construction features such as slot harmonics or rotor eccentricity. Regarding the simulation, the PMSM is fed by a 3-phase two-level sinusoidal PWM VSC, operating at constant switching frequency $f_{sw} = 5$ [kHz] and with linear modulation. As it is well known, with a high switching frequency there are no low-order voltage harmonics in the machine voltage spectrum. For this reason, the low-order voltage harmonics at h_{13} and h_5 are artificially added to the machine terminals to induce torsional vibrations and to allow analyzing specific system operating conditions. It is remarked that the scope of this paper is to test the ability of the presented observer in providing a good estimate of the torsional vibrations, when present. The simulation is divided into three stages:

- First, the system is accelerated from standstill to the steady state mechanical speed $\omega_m^{res,h_{13}}$;
- Second, a harmonic voltage of order h_{13} is injected for a short-time-interval and the observer performance at mechanical resonance is evaluated;
- Finally, a harmonic voltage of order h_5 leading to low-amplitude torsional vibrations is injected for a

short-time-interval, evaluating the observer in this condition too.

The speed trends in this simulation are shown in Fig. 3: between simulation time $t = 140 \div 145 s$ a voltage harmonic of order h_{13} is injected, leading to mechanical resonance. Indeed, the PMSM mechanical angular speed ω_m presents a high oscillation with respect to ω_L, which is characterized by low oscillations due to $J_L \gg J_m$. The voltage harmonic of order h_5 is injected in $t = 145 \div 150 s$, producing low amplitude vibrations, as can be seen from ω_m and ω_L trends.

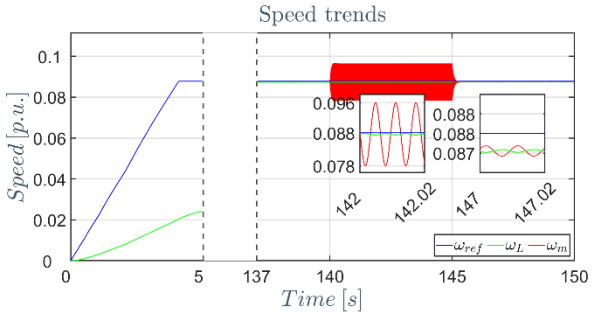

Fig. 3. Reference-, PMSM- and Load- mechanical angular speed; two voltage harmonics are injected: one (t=140÷145s) leading to a mechanical resonance, one (t=145÷150s) creating low-amplitude torsional vibrations;

The magnitude of the voltage harmonics is selected to be 15 percent of the voltage fundamental harmonic at $\omega_m^{res,h_{13}}$, to properly excite the torsional phenomena. To extract the oscillating component from each system inputs and outputs, a High-Pass (HP) filter is used, with cut-off angular frequency $\omega_{co,HP} = 0.1\,\Omega_{res}$. Regarding the system inputs, the control reference stator voltages oscillating components are used. The parameters used in the simulation are listed in TABLE II. The weights applied to each non-measured state estimate (listed in TABLE IV) are chosen to minimize the estimation errors at $\omega_m^{res,h_{13}}$ in the presence of a torque harmonic related to the h_{13} voltage harmonic injection. In particular, $K = 512$ samples, with a time-step equal to h_{step}, are acquired starting from $t = 142\ s$. In this way, the samples span for several periods $T_{res} = 2\pi/\Omega_{res}$, guaranteeing the acquisition of useful information of the observation errors oscillating at Ω_{res}.

B. *Simulation results*

The observer performance is evaluated by assessing its accuracy in estimating the shaft torque $T_{sh} = K_{sh}(\theta_m - \theta_L)$. In this case, the overall system provides the estimates of the oscillating components of the state variables, i.e. $\boldsymbol{\Delta x}$, thus only the oscillating component of the shaft torque $\Delta T_{sh} = K_{sh}(\Delta\theta_m - \Delta\theta_L)$ can be retrieved. For this reason, the first simulation stage is not relevant for the performance evaluation because there are no harmonics exciting vibrations. Fig. 4 shows the comparison between the estimated value $\Delta\hat{T}_{sh}$ and the true one ΔT_{sh}, normalized to $T_{n,m}$. Fig. 5 shows the trend of the shaft torque observation error, normalized to $T_{n,m}$. The shaft torque observation error at resonance, so as concerns the h_{13} voltage harmonic injection, is rather low, as a result of both suitable observer design and proper weights choice. ΔT_{sh} and $\Delta\hat{T}_{sh}$ are in phase, with a peak error at steady state of 0.05 p.u., with respect to the ΔT_{sh} peak value of approximately 0.40 p.u., corresponding to a maximum observation error of approximately 12.5% to the real value. On the other hand, the observer performance is slightly worse when a generic voltage disturbance of order h_5 is injected, with a steady-state peak value of the shaft torque observation error of approximately 0.01 p.u. against a ΔT_{sh} peak value of 0.02 p.u., thus leading to a 50% of maximum observation error with respect to the true value. Also in this case ΔT_{sh} and $\Delta\hat{T}_{sh}$ are in phase with respect to each other. From Fig. 4, two overshoots can be seen at $t = 140\ s$, relatively low in amplitude, and at $t = 145\ s$, much greater. These are related to the sudden change of the disturbance injected: however, the NESO rapidly damps these overshoots reaching a new steady state condition.

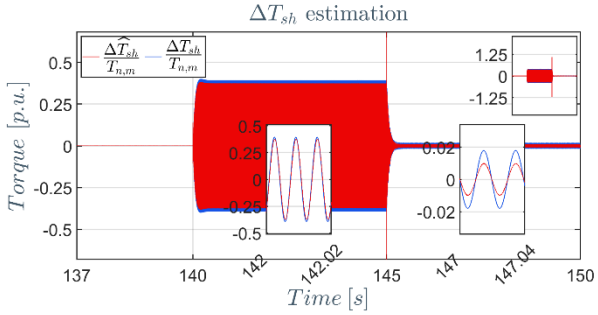

Fig. 4. Shaft torque oscillating component real value ΔT_{sh} and estimated value $\Delta\hat{T}_{sh}$; the observation accuracy is higher in mechanical resonance with respect to the low-amplitude torsional vibrations condition.

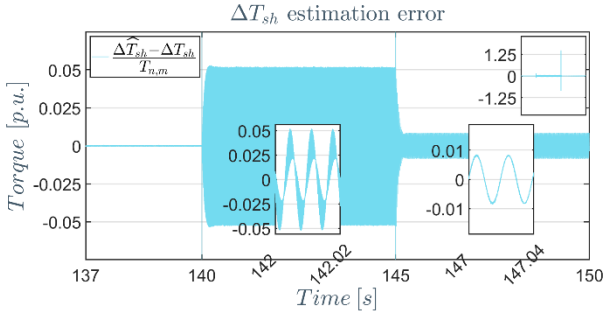

Fig. 5. Shaft torque oscillating component observation error; the observation accuracy is higher in mechanical resonance with respect to the low-amplitude torsional vibrations condition.

V. Conclusion

In this paper, an NESO was designed and analyzed for a two-degree-of-freedom PMSM drive system, modeled comprising both the mechanical and the electrical dynamics. A detailed and reproducible step-by-step methodology on the observer design was presented. The aim was to estimate the torsional vibrations that arise in the system at mechanical resonance. The observer performance was analyzed by assessing its ability to estimate the shaft torque under different operating conditions. The results showed that the proposed observer provides a good estimation of the shaft torque oscillating component at mechanical resonance, thus with strong torsional vibrations, while its performance decreases when low-amplitude torsional oscillations are present. Further research is needed to:

- Assess the effectiveness of the presented observers in an experimental setup, with both measurements subjected to noises and the system parameters variability;

- Improve the weights definition method for the NESO, for example, considering using different sets of weights depending on the operating conditions or operating speeds.

VI. Appendix I

The following steps are needed to transform the generic Subsystem i (8) into the realization of the observability canonical form (9):

1) find system (8) transfer function matrix: $\boldsymbol{W_i}(s) = \boldsymbol{C_{\Delta i}}(s\boldsymbol{I} - \boldsymbol{A_{\Delta i}})^{-1}\boldsymbol{B_{\Delta i}}$;

2) find the minimum polynomial $qW_i(s) = s^{n_i} + \sum_{i=0}^{n_i-1}\gamma_i s^i$ of $\boldsymbol{W_i}(s)$, defined as the common denominator of the elements of $\boldsymbol{W_i}(s)$, after all the simplifications of common terms of its rational terms;

3) Considering the coefficients of polynomial $qW_i(s)$, build $\boldsymbol{A_{zi}}$ as:

$$\boldsymbol{A_{zi}} = \begin{bmatrix} 0 & 1 & 0 & \dots & 0 & 0 \\ 0 & 0 & 1 & \dots & 0 & 0 \\ \dots & \dots & \dots & \dots & \dots & \dots \\ 0 & 0 & 0 & \dots & 0 & 1 \\ -\gamma_1 & -\gamma_2 & -\gamma_3 & \dots & -\gamma_{n_i-2} & -\gamma_{n_i-1} \end{bmatrix} \in R^{n_i x n_i};$$

4) Define $\boldsymbol{W_0}(s) = \boldsymbol{W_i}(s)$ and $\overline{\boldsymbol{W}}_{\boldsymbol{0}} = \lim_{s\to\infty} \boldsymbol{W_0}(s)$, and given $1 \le h \le n_i$, define $\boldsymbol{W_h}(s) = s(\boldsymbol{W_{h-1}}(s) - \overline{\boldsymbol{W}}_{\boldsymbol{h-1}})$ and $\overline{\boldsymbol{W}}_{\boldsymbol{h}} = \lim_{s\to\infty} \boldsymbol{W_h}(s)$;

5) Build: $\boldsymbol{B_{zi}} = \left[\overline{\boldsymbol{W}}_{\boldsymbol{1}}\ \overline{\boldsymbol{W}}_{\boldsymbol{2}}\ \dots\ \overline{\boldsymbol{W}}_{n_i}\right]^T \in R^{n_i xp}$;

6) Find the controllability matrix of system (8) using only one column of $\boldsymbol{B_{\Delta i}} = [\boldsymbol{B_{\Delta i,1}}\ \boldsymbol{B_{\Delta i,2}} \dots \boldsymbol{B_{\Delta i,p}}]$, for example column 1 $\boldsymbol{B_{\Delta i,1}}$:
$\boldsymbol{P_i} = [\boldsymbol{B_{\Delta i,1}}\ \boldsymbol{A_{\Delta i}}\boldsymbol{B_{\Delta i,1}}\ \boldsymbol{A_{\Delta i}^2}\boldsymbol{B_{\Delta i,1}}\ \dots\ \boldsymbol{A_{\Delta i}^{n_i}}\boldsymbol{B_{\Delta i,1}}]$;

7) Find the controllability matrix of system (9) using only one column of $\boldsymbol{B_{zi}} = [\boldsymbol{B_{zi,1}}\ \boldsymbol{B_{zi,2}} \dots \boldsymbol{B_{zi,p}}]$, for example column 1 $\boldsymbol{B_{zi,1}}$:
$\boldsymbol{P_{zi}} = [\boldsymbol{B_{zi}}\ \boldsymbol{A_{zi}}\boldsymbol{B_{zi}}\ \boldsymbol{A_{zi}^2}\boldsymbol{B_{zi}}\ \dots\ \boldsymbol{A_{zi}^{n_i}}\boldsymbol{B_{zi}}]$;

8) Find $\boldsymbol{T_i} = \boldsymbol{P_{zi}} * \boldsymbol{P_i^{-1}}$ and check $det\,\boldsymbol{T_i} \neq 0$; if not, change column of $\boldsymbol{B_{\Delta i}}$ and $\boldsymbol{B_{zi}}$.

VII. Appendix II

TABLE I. System mechanical and electrical parameters

PMSM	
$P_{n,m}$[W],$V_n^{ph.}$[V], I_n [A], pp	6910, 174.7, 14.8, 3
R_s [Ω], L_s [mH]	0.393, 4.8
Ψ_{PM} [Vs], $\Psi_{PM,q}$ [Vs]	0.165, $\sqrt{3}$·0.165
J_m [kgm^2], H_m [s]	$3.02 * 10^{-3}$, 0.022
$\Omega_{n,m}$[rad/s], Ω_{res}[rad/s]	314.16, 992.65
Load and shaft	
J_L[kgm^2], $T_{n,L}$ [Nm]	0.122, 47.75
H_L [s], K_L[Nms], K_{sh} [Nm/rad]	0.401, 0.315, 2902

TABLE II. Simulation PI and control parameters

PI and control parameters	
$f_{co,\Omega}$[Hz], $f_{co,I}$ [Hz], h_{step}[μs]	0.1, 300, 100

TABLE III. Subsystems' NESO β-coefficients

Subsystem 1		Subsystem 2 and 3	
β_1	$4.24 * 10^4$	β_1	$3.63 * 10^4$
β_2	$7.99 * 10^8$	β_2	$5.70 * 10^8$
β_3	$8.37 * 10^{12}$	β_3	$4.78 * 10^{12}$
β_4	$5.26 * 10^{16}$	β_4	$2.25 * 10^{16}$
β_5	$1.98 * 10^{20}$	β_5	$5.66 * 10^{19}$
β_6	$4.15 * 10^{23}$	β_6	$5.93 * 10^{22}$
β_7	$3.73 * 10^{26}$		

TABLE IV. NESO estimates' weights

$\boldsymbol{w}_x = [\boldsymbol{w_1}, \boldsymbol{w_2}, \boldsymbol{w_3}]_x$	
$\boldsymbol{w}_{\Delta\theta_L}$	$[-1, -0.1, 0.025]$
$\boldsymbol{w}_{\Delta\omega_m}$	$[1, 0, 0]$
$\boldsymbol{w}_{\Delta\omega_L}$	$[-1, 0.025, 0]$

References

[1] R. M. Pindoriya, R. K. Thakur, B. S. Rajpurohit, and R. Kumar, 'Numerical and experimental analysis of torsional vibration and acoustic noise of PMSM coupled with DC generator', *IEEE Trans. Ind. Electron.*, vol. 69, no. 4, pp. 3345–3356, 2022.

[2] M. Bruha, M. Byrtus, K. Pietiläinen, M. Rossi, and M. Mauri, 'Torsional issues related to variable frequency control of elastic drive systems', in *IECON 2016 - 42nd Annual Conf. of the IEEE Ind. Electron. Soc.*, pp. 2981–2987.

[3] A. Arkkio, S. Cederström, H. A. A. Awan, S. E. Saarakkala, and T. P. Holopainen, 'Additional losses of electrical machines under torsional vibration', *IEEE Trans. En. Conv.*, vol. 33, no. 1, pp. 245–251, 2018.

[4] J. Song-Manguelle, G. Ekemb, D. L. Mon-Nzongo, T. Jin, and M. L. Doumbia, 'A theoretical analysis of pulsating torque components in AC machines with variable frequency drives and dynamic mechanical loads', *IEEE Trans. Ind. El.*, vol. 65, no. 12, pp. 9311–9324, 2018.

[5] S. H. Kia, H. Henao, and Gé.-A. Capolino, 'Torsional vibration assessment using induction machine electromagnetic torque estimation', *IEEE Trans. Ind. El.*, vol. 57, no. 1, pp. 209–219, 2010.

[6] D. Pejovski, A. D. Gerlando, G. M. Foglia, M. F. Iacchetti, and R. Perini, 'Current harmonics in surface-mounted PMSM electrical drive for monitoring torsional vibrations', *IEEE Trans. Ind. Appl.*, pp. 1–10, 2024, DOI: 10.1109/TIA.2024.3357622 .

[7] X. Shi, J. Shao, J. Si, and B. Li, 'Experiment and simulation of rotor's torsional vibration based on sensorless detection technology', in *2008 IEEE Int. Conf. on Autom. and Logistics*., pp. 2673–2678.

[8] C. Bruzzese and E. Santini, 'Rotor torsional resonance detection in induction drives by MCSA focused on rotor slot harmonics', in *2017 AEIT Int. Annual Conf.*, pp. 1–6.

[9] W. Wang and Z. Gao, 'A comparison study of advanced state observer design techniques', in *Proc. of the 2003 American Control Conf., 2003*, pp. 4754–4759 vol.6.

[10] A.-I. Szedlak-Stinean, R.-E. Precup, R.-C. Roman, E. M. Petriu, C.-A. Bojan-Dragos, and E.-L. Hedrea, 'Discrete-time linear and nonlinear observers for an electromechanical plant with state feedback control', in *2022 IEEE Symp. Series on Computational Intelligence (SSCI)*, pp. 700–707.

[11] H. K. Khalil, *Nonlinear Systems*, Third. Prentice-Hall, 2002.

[12] B.-Z. Guo and Z. Zhao, *Active Disturbance Rejection Control for Nonlinear Systems: An Introduction*. 2016.

[13] H. Li, H. Xu, X. Chen, P. Zhou, C. Gong, and Y. Qin, 'Design of current and back electromotive force observers for ironless-stator permanent magnet brushless DC motor dual-stage drive', in *2023 26th Int.Conf. on El. Mach. and Systems (ICEMS)*, pp. 41–46.

[14] B. Liu, J. Zhao, Q. Huang, F. Milano, and W. Hu, 'Robust nonlinear controller to damp drivetrain torsional oscillation of wind turbine generators', *IEEE Trans. Sust. En.*, vol. 12, no. 2, pp. 1336–46, 2021.

[15] R. C. Dorf and R. H. Bishop, *Modern Control Systems*. Pearson Prentice Hall, 2008.

[16] P. J. Antsaklis, *Linear systems*. New York: McGraw-Hill, 1997.